Phonon-assisted luminescence of polar semiconductors: Fröhlich coupling versus deformation-potential scattering

A. Chernikov, V. Bornwasser, M. Koch, S. Chatterjee, C. N. Böttge, T. Feldtmann, M. Kira, and S. W. Koch
Faculty of Physics and Materials Sciences Center, Philipps-Universität Marburg, Renthof 5, D-35032 Marburg, Germany

T. Wassner
Walter Schottky Institut, Technische Universität München, Am Coulombwall 3, D-85748 Garching, Germany

S. Lautenschläger, B. K. Meyer, and M. Eickhoff
I. Physikalisches Institut, Justus-Liebig-Universität Gießen, Heinrich-Buff-Ring 16, D-35392 Gießen, Germany
(Received 1 August 2011; published 4 January 2012)

The origin of exciton-phonon interaction in polar semiconductors is investigated. The relative contributions of Fröhlich coupling and deformation potential scattering are identified by analyzing experimentally measured phonon-assisted luminescence using a rigorous many-body approach. Our experiment-theory comparison demonstrates that phonon scattering is significantly influenced by many-body interactions. Fröhlich interaction can be strongly suppressed for excitons even when it dominates electronic single particle scattering. The results show that deformation potential scattering dominates the exciton-phonon interaction in ZnO, whereas Fröhlich interaction prevails in CdS, and both coupling mechanisms yield almost equal contributions in ZnS.

DOI: 10.1103/PhysRevB.85.035201 PACS number(s): 78.47.jd, 63.20.kk, 78.55.Et

I. INTRODUCTION

Scattering between charge carriers and lattice vibrations is one of the elementary interactions in semiconductors. The microscopic understanding of this process is crucial for the analysis of a wide range of phenomena like cooling of a hot carrier system,[1–3] light–matter interaction,[4,5] and dephasing of coherent excitations,[6–8] to name only a few. Fröhlich interaction is presumably the most prominent carrier-phonon scattering mechanism.[9–11] It involves the direct coupling of the polarization of the lattice vibrations to the electron charge [Fig. 1(a)]. The dependence of the coupling strength on the quasimomentum **k** is qualitatively shown by the dark-gray area in Fig. 1(c). This interaction decays for large **k** and is, therefore, most efficient at transferring small momenta between electrons and phonons. In inorganic semiconductors, Fröhlich scattering is known to be of central importance in compound materials such as GaAs and GaP with polar contributions to atomic bonds,[12,13] and it is particularly strong in wide-gap materials, like CdS, ZnO, and GaN. Additionally, Fröhlich interaction is commonly applied to describe surface-related phonon scattering,[14] vibrational properties of low-dimensional systems,[15] and coupling to polarons.[16,17]

Generally, carrier-phonon interaction has to be considered in the presence of carrier-carrier Coulomb scattering. This leads to the formation of electron hole pairs, i.e., excitons,[18] observed in a wide range of materials such as organic and anorganic semiconductors,[13,19] polymers,[20] and many more. Also, in the case of the excitons, the Fröhlich interaction is commonly used to describe coupling to phonons.[21–24] However, the attractive electron-hole interaction should introduce significant modifications to the phonon scattering. While the Fröhlich coupling is strong for a single carrier, it may be much less efficient for a correlated many-body state. Thus, polar interaction between phonons and excitons should be at least partially canceled due to the opposite charges of electrons and holes within excitons. Indications for this behavior are observed and suggested in previous literature studies, e.g., on exciton-phonon scattering in confined quantum-dot systems.[25–27]

A second carrier-phonon scattering mechanism is based on the deformation of the atomic lattice by a phonon, leading to the indirect interaction with an electron via the modulations of the periodic lattice potential. This process is known as deformation potential scattering.[13,28,29] It dominates the electron-phonon coupling in nonpolar materials like Si or Ge.[12,30] The strength of the deformation potential scattering is essentially constant in **k** and leads to a relatively weak dependence of the coupling on the transferred momentum, see Fig. 1(c). Nevertheless, for small **k** values, the absolute interaction strength is considerably smaller compared to the Fröhlich interaction. However, this nonpolar coupling is only marginally changed for excitons or other correlated many-body states compared with the individual carrier interaction.

In this paper, we investigate the exciton-phonon scattering in three different polar semiconductors that are known for strong Fröhlich interaction between single charge carriers and phonons. We demonstrate that phonon scattering is significantly influenced by many-body interactions. Surprisingly, the Fröhlich coupling can be partially or even completely suppressed for exciton-phonon interactions, leaving deformation potential scattering as the dominant mechanism.

We have studied the phonon-assisted luminescence in order to identify the nature of the exciton-phonon interaction. This process is shown schematically in Fig. 1(d) in the polaron picture. The radiative recombination of excitons leads to the so-called zero-phonon line (ZPL) in the emission spectrum. The phonon-assisted radiative recombination, i.e., the simultaneous emission of a photon and one or several optical phonons, yields additional distinct spectral signatures, the so-called phonon sidebands (PSBs).[31,32] We exploit the differences between the two coupling mechanisms with respect to the interaction strength dependence on the transferred momentum by altering the carrier distribution in the reciprocal

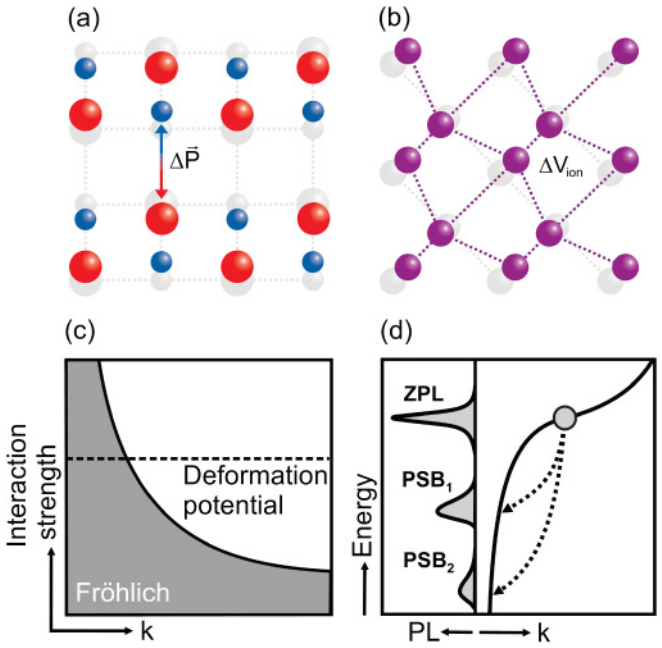

FIG. 1. (Color online) Schematic illustration of electron-phonon interaction mechanisms: polar Fröhlich coupling (a) and deformation potential scattering (b). The corresponding interaction strength is shown in (c) as a function of transferred quasimomentum **k**. Sketch of a phonon-sideband emission process in the polaron picture (d): The lower polariton branch is plotted on the right-hand side, the photoluminescence spectrum on the left.

space. Investigating the temperature dependence of the relative sideband ratios thus allows us to identify the role of Fröhlich versus deformation potential contributions to the exciton-phonon scattering processes.

II. THEORY

The Fröhlich-type carrier-LO phonon interaction stems from the relative displacements of oppositely charged ions within a unit cell, which produces a macroscopic polarization

$$\mathbf{P}(\mathbf{r}) = \frac{\hbar\Omega_{\mathrm{LO}}\epsilon_0}{e}\sum_{\mathbf{p}} g_{\mathbf{p}}^{\lambda}\frac{\mathbf{p}}{|\mathbf{p}|}\,\mathrm{e}^{\mathrm{i}\,\mathbf{p}\cdot\mathbf{r}}(D_{\mathbf{p}} - D_{-\mathbf{p}}^{\dagger}). \tag{1}$$

Here, $\frac{\mathbf{p}}{|\mathbf{p}|}(D_{\mathbf{p}} - D_{-\mathbf{p}}^{\dagger})$ describes the quantized form of induced displacement containing the Boson creation and annihilation operators $D_{\mathbf{p}}^{\dagger}$ and $D_{\mathbf{p}}$ for phonons with wave vector **p**. The associated polarization creates a macroscopic field via a Coulombic term. It is customary to express this via the band-independent Fröhlich matrix element[9]

$$\left|g_{\mathbf{p}}^{\lambda}\right|^2 = \frac{e^2}{\epsilon_0\mathcal{L}^3 2\hbar\Omega_{\mathrm{LO}}}\frac{1}{|\mathbf{p}|^2}\left[\frac{1}{\varepsilon(\infty)} - \frac{1}{\varepsilon(0)}\right], \quad \lambda = \{\mathrm{c},\mathrm{v}\}, \tag{2}$$

where c and v represent conduction and valence band, respectively, and $\mathcal{L}^3$ is the normalization volume while ϵ_0 denotes the vacuum permittivity. It is also convenient to include dielectric constants for both high-frequency $\varepsilon(\infty)$ and low-frequency $\varepsilon(0)$ into $g_{\mathbf{p}}^{\lambda}$. The transferred momentum between the electron and LO phonon is denoted by **p**, and $\hbar\Omega_{\mathrm{LO}}$ is the respective energy of the phonon. These lattice vibrations couple with λ electrons having momentum **k**, which is described by the phonon-carrier interaction

$$H_{\mathrm{phon}} = \hbar\Omega_{\mathrm{LO}}\sum_{\lambda,\mathbf{k},\mathbf{p}} g_{\mathbf{p}}^{\lambda}\,a_{\lambda,\mathbf{k}-\mathbf{p}}^{\dagger}a_{\lambda,\mathbf{k}}(D_{-\mathbf{p}} - D_{\mathbf{p}}^{\dagger}), \tag{3}$$

where $a_{\lambda,\mathbf{k}}$ is a Fermion operator describing carriers.

The deformation-potential coupling originates from the variations of the bond lengths and angles that locally change the electronic band energies and lead to strongly band-dependent matrix elements. The resulting carrier-phonon interaction has the same form as Eq. (3); one just needs to replace $g_{\mathbf{p}}^{\lambda}$ by the deformation potential matrix element[33]

$$|g^{\lambda,\mathrm{def}}|^2 = \frac{1}{2\rho\mathcal{L}^3\hbar\Omega_{\mathrm{LO}}^3}\frac{(M_1+M_2)^2}{2M_1M_2}\frac{|d^{\lambda}|^2}{a^2}, \tag{4}$$

where ρ is the density of the material, M_1 and M_2 are the masses of the two different base atoms, d^{λ} is the optical deformation potential constant, and a is the lattice parameter.

In general, the deformation potentials are strongly band dependent. It can be shown that there is no deformation-potential interaction between conduction-band electrons and optical phonons in direct semiconductors, based on symmetry.[12,34] Therefore, d^{c} vanishes while d^{v} has a finite value in the range of some 10 eV and is also often denoted as $d_0 \equiv d^{\mathrm{v}}$ in the literature. The authors of Ref. 35 have used a tight-binding approach to calculate the deformation potentials for several semiconductors in diamond and zincblende structures and obtained a value of $d^{\mathrm{v}} = 39.8$ eV for ZnO and $d^{\mathrm{v}} = 23.7$ eV for CdS. The respective values must be converted from zincblende- to wurtzite-structure parameters for the comparison to our experimental data. These are derived using the relations of Ref. 36 where the authors have presented a general derivation of the deformation potentials in zincblende- and wurtzite-type semiconductors as well as a relation that connects both systems. The coupling constants for optical deformation potential scattering used in this work are $d_{\mathrm{ZnO}}^{\mathrm{v}} = 49.7$ eV and $d_{\mathrm{CdS}}^{\mathrm{v}} = 29.6$ eV.

The phonon sideband emission stems from phonon-assisted three-particle correlations that are systematically included with the semiconductor luminescence equations[37] as presented in the appendix. The resulting steady-state luminescence spectrum in free space follows from photon flux that is proportional to

$$I_{\mathrm{PL}}(\omega) = I_{\mathrm{ZPL}}(\omega) + I_{\mathrm{PSB}_1}(\omega) + I_{\mathrm{PSB}_2}(\omega), \tag{5}$$

where the ZPL, PSB_1, and PSB_2 contributions are simply summed over. When the 1*s*-exciton populations dominate over electron-hole plasma sources,[38] the ZPL spectrum follows from

$$I_{\mathrm{ZPL}}(\omega) = \mathrm{Im}\left[\frac{N_{\mathrm{ZPL}} - \delta N_{\mathrm{ZPL}}^{(1)} - \delta N_{\mathrm{ZPL}}^{(2)}}{E_{1s,\mathbf{0}} - \hbar\omega - \mathrm{i}\gamma_0}\right], \tag{6}$$

where the strength of the 1*s* emission —as in the case of our experiment— is defined by the exciton population $\Delta N_{1s,\mathbf{p}}$ at the vanishing momentum, i.e.,

$$N_{\mathrm{ZPL}} = \Delta N_{1s,\mathbf{0}}. \tag{7}$$

The emerging sidebands yield further corrections

$$\delta N^{(1)}_{\mathrm{ZPL}} = \sum_{\mathbf{Q}} \left| \frac{G^{1s,1s}_{\mathbf{Q}}}{\hbar\Omega - E^{\mathrm{CoM}}_{\mathbf{Q}}} \right|^2 \Delta N_{1s,\mathbf{Q}}, \tag{8}$$

$$\delta N^{(2)}_{\mathrm{ZPL}} = -\sum_{\mathbf{Q},\mathbf{p}} \sum_{\nu,\nu'} \frac{G^{1s,\nu}_{\mathbf{p}} G^{\nu,1s}_{\mathbf{Q}-\mathbf{p}}\, \Delta N_{1s,\mathbf{Q}}}{\left(2\hbar\Omega - E^{\mathrm{CoM}}_{\mathbf{Q}}\right)^2 \Delta E^{\nu,1s}_{\mathbf{p},\mathbf{0}}} \times \left[\frac{\left(G^{1s,\nu'} G^{\nu',1s}_{\mathbf{Q}-\mathbf{p}}\right)^*}{\Delta E^{1s,\nu'}_{\mathbf{Q},\mathbf{p}}} + \frac{\left(G^{1s,\nu'}_{\mathbf{Q}-\mathbf{p}} G^{\nu',1s}_{\mathbf{p}}\right)^*}{\Delta E^{1s,\nu'}_{\mathbf{Q},\mathbf{Q}-\mathbf{p}}} \right]. \tag{9}$$

$\Delta N_{1s,\mathbf{q}}$ defines the center-of-mass distributions of $1s$ excitons and is assumed to follow the Bose-Einstein distribution. The corresponding exciton energy $E_{\nu,\mathbf{Q}} = E_\nu + \frac{\hbar^2\mathbf{Q}^2}{2M}$ is a sum of the exciton eigenenergy E_ν and the center-of-mass energy $E^{\mathrm{CoM}}_{\mathbf{Q}} = \frac{\hbar^2\mathbf{Q}^2}{2M}$ with the total electron-hole mass $M = m_{\mathrm{e}} + m_{\mathrm{h}}$. We also have identified the transition energy

$$\Delta E^{\nu,\nu'}_{\mathbf{Q},\mathbf{p}} \equiv \hbar\Omega - E_{\nu,\mathbf{Q}} + E_{\nu',\mathbf{p}}, \tag{10}$$

between the exciton state $(\nu,\mathbf{Q})$ and phonon-assisted transition to the exciton state $(\nu',\mathbf{p})$.

The exciton-phonon matrix elements are defined by

$$G^{\nu,\nu'}_{\mathbf{p}} = \hbar\Omega_{\mathrm{LO}} \sum_{\mathbf{k}'} \phi_\nu(\mathbf{k}' + \mathbf{p}_{\mathrm{e}}) \left[g^{\mathrm{c}}_{\mathbf{p}}\, \phi_{\nu'}(\mathbf{k}' + \mathbf{p}) - g^{\mathrm{v}}_{\mathbf{p}}\, \phi_{\nu'}(\mathbf{k}') \right]^\star, \tag{11}$$

where $\mathbf{p}_{\mathrm{e}} = \frac{m_{\mathrm{e}}}{m_{\mathrm{e}}+m_{\mathrm{h}}}\mathbf{p}$ and $\phi_\nu(\mathbf{k})$ is the low-density exciton wave function. In case phonon-matrix elements for the conduction and valence bands are equal—as it is for the Fröhlich interaction—Eq. (11) becomes

$$G^{\mathrm{Fröhlich}}_{\mathbf{p}} = \hbar\Omega_{\mathrm{LO}} g_{\mathbf{p}} \sum_{\mathbf{k}'} \phi_\nu(\mathbf{k}' + \mathbf{p}_{\mathrm{e}}) [\phi_{\nu'}(\mathbf{k}' + \mathbf{p}) - \phi_{\nu'}(\mathbf{k}')]^\star. \tag{12}$$

This easily shows that one observes only a weak Fröhlich contribution of the phonon interaction especially for small phonon momenta $\mathbf{p}$. Since deformation potential has $d^{\mathrm{c}} = 0$ and $d^{\mathrm{v}} \neq 0$, it does not produce a reduction of phonon interaction for excitons. Therefore, the Fröhlich interaction couples excitons with phonons less efficiently than the deformation potential does.

We see from Eq. (6) that N_{ZPL} defines the strength of ZPL emission with phonon-assisted processes. Therefore, $\delta N^{(1)}_{\mathrm{ZPL}}$ and $\delta N^{(2)}_{\mathrm{ZPL}}$ provide corrections due to the presence of higher-order phonon-assisted processes. Since the ZPL is several orders of magnitude larger than the phonon sidebands, the introduced corrections have only a very slight influence on the ZPL emission. Furthermore, the energy denominators in Eqs. (8) and (9) depend only weakly on the phonon momenta, because the optical phonon energy is large compared with the energetic distance between the relevant excitonic resonances. It can be shown that the (ν,ν') combinations $(1s,1s)$ and $(1s,2p)$ especially show a significant scattering probability $|G^{\nu,\nu'}_{\mathbf{p}}|^2$.[39]

The phonon-sideband contributions up to the second sideband are similar to Eq. (6):

$$I_{\mathrm{PSB}_1}(\omega) = \mathrm{Im}\left[\sum_{\mathbf{Q}} \frac{N_{\mathrm{PSB}_1,\mathbf{Q}} - \delta N^{(2)}_{\mathrm{PSB}_1,\mathbf{Q}}}{E_{1s,\mathbf{Q}} - \hbar\Omega - \hbar\omega - \mathrm{i}\gamma_1} \right], \tag{13}$$

$$I_{\mathrm{PSB}_2}(\omega) = \mathrm{Im}\left[\sum_{\mathbf{Q}} \frac{N_{\mathrm{PSB}_2,\mathbf{Q}}}{E_{1s,\mathbf{Q}} - 2\hbar\Omega - \hbar\omega - \mathrm{i}\gamma_2} \right]. \tag{14}$$

The magnitude of the PSB resonances are defined by

$$N_{\mathrm{PSB}_1,\mathbf{Q}} = \left| \frac{G^{1s,1s}_{\mathbf{Q}}}{\hbar\Omega - E^{\mathrm{CoM}}_{\mathbf{Q}}} \right|^2 \Delta N_{1s,\mathbf{Q}}, \tag{15}$$

$$\delta N^{(2)}_{\mathrm{PSB}_1,\mathbf{Q}} = \sum_{\mathbf{p}} \frac{G^{1s,1s}_{\mathbf{Q}} G^{1s,1s}_{\mathbf{p}}\, \Delta N_{1s,\mathbf{Q}+\mathbf{p}}}{\left(2\hbar\Omega - E^{\mathrm{CoM}}_{\mathbf{Q}+\mathbf{p}}\right)\left(\hbar\Omega - E^{\mathrm{CoM}}_{\mathbf{Q}}\right) \Delta E^{1s,1s}_{\mathbf{Q}+\mathbf{p},\mathbf{Q}}} \times \sum_{\nu} \left[\frac{\left(G^{1s,\nu}_{\mathbf{Q}} G^{\nu,1s}_{\mathbf{p}}\right)^*}{\Delta E^{1s,\nu}_{\mathbf{Q}+\mathbf{p},\mathbf{Q}}} + \frac{\left(G^{1s,\nu}_{\mathbf{p}} G^{\nu,1s}_{\mathbf{Q}}\right)^*}{\Delta E^{1s,\nu}_{\mathbf{Q}+\mathbf{p},\mathbf{p}}} \right], \tag{16}$$

$$N_{\mathrm{PSB}_2,\mathbf{Q}} = \sum_{\mathbf{p}} \sum_{\nu,\nu'} \frac{G^{1s,\nu}_{\mathbf{p}} G^{\nu,1s}_{\mathbf{Q}-\mathbf{p}}\, \Delta N_{1s,\mathbf{Q}}}{\left(2\hbar\Omega - E^{\mathrm{CoM}}_{\mathbf{Q}}\right)^2 \Delta E^{1s,\nu}_{\mathbf{Q},\mathbf{p}}} \times \left[\frac{\left(G^{1s,\nu'}_{\mathbf{p}} G^{\nu',1s}_{\mathbf{Q}-\mathbf{p}}\right)^*}{\Delta E^{1s,\nu'}_{\mathbf{Q},\mathbf{p}}} + \frac{\left(G^{1s,\nu'}_{\mathbf{Q}-\mathbf{p}} G^{\nu',1s}_{\mathbf{p}}\right)^*}{\Delta E^{1s,\nu'}_{\mathbf{Q},\mathbf{Q}-\mathbf{p}}} \right]. \tag{17}$$

It is straightforward to show that the total PL, $\int I_{\mathrm{PL}}(\omega)\,\mathrm{d}\omega$, is not altered by the phonon-assisted processes. Therefore, $\delta N^{(1)}$ and $\delta N^{(2)}$ in Eqs. (6) and (13)–(14) just redistribute emission among the ZPL and PSBs through the phonon-assisted processes.

We also see from Eqs. (6)–(9) that phonon-assisted contributions change the ZPL via both $\delta N^{(1)}_{\mathrm{ZPL}}$ and $\delta N^{(2)}_{\mathrm{ZPL}}$ stemming from single- and two-phonon assisted processes, respectively. At the same time, the PSB_2 alters the PSB_1 via the $\delta N^{(2)}_{\mathrm{PSB}_1,\mathbf{Q}}$ contribution. The PSB_2 itself has only one phonon-assisted scattering source $N_{\mathrm{PSB}_2,\mathbf{Q}}$, since we include effects up to the second sideband, see Appendix A. Both the PSB_1 and PSB_2 spectra consist of a sum over exciton momentum in the Lorentzians. Therefore, the PSBs exhibit a broader spectrum at the high-energy tail than the ZPL. In particular, the slope of the high energy flank of the PSB_1 reflects the momentum-dependence of the carrier-phonon interaction, temperature of the system, available phase-space for the scattering process, and the dephasing constant γ_0. Due to nontrivial mixing of these effects, this slope is generally different for various PSBs. Therefore, the carrier temperature cannot be extracted from the fitting of the high-energy tail of a PSB by the Boltzmann function.

The intensities of PSB_1 and PSB_2 depend on the phonon-matrix elements G in the second and fourth power, respectively. Thus, the ratio between PSB_2 and PSB_1 emission is determined by the carrier temperature and by the dependence of G on the transferred momentum. As a result, one expects the $\mathrm{PSB}_2/\mathrm{PSB}_1$ ratio to decrease with increasing temperature for the momentum-dependent Fröhlich interaction since the corresponding phonon-matrix elements decrease for increasing momenta, c.f. Fig. 1. In the case of the momentum-free deformation potential, however, the phonon-matrix elements

are independent of the **p** and **Q** sums and become constant factors in Eqs. (15)–(17). Hence, the ratio PSB_2/PSB_1 does not depend on the transferred momenta and, therefore, on carrier temperature. Consequently, we expect a strongly temperature-dependent second-to-first sideband ratio for the Fröhlich scattering mechanism, while PSB_2/PSB_1 remains constant if deformation-potential coupling prevails. Thus, the carrier temperature dependence of the PSB-emission ratios offers an experimentally accessible method to identify the nature of the exciton-phonon interaction. In an experiment, the carrier temperature is easily controlled via lattice temperature and/or the excitation conditions.

III. EXPERIMENT

We perform lattice temperature-dependent measurements of the first and second PSB emission spectra for three different materials: ZnO, ZnS, and CdS. These are typical representatives for polar wide-gap semiconductors exhibiting strong electron-phonon and Coulomb-interaction effects.[12,13,32] The ZnO and ZnS samples are epitaxially grown 0.3-μm and 1-μm layers, respectively; for CdS, a chemically synthesized flake of about 10-μm thickness is investigated. Applying short-pulse interband excitation, we measure the time-resolved PL to ensure that only incoherent emission sources contribute to the signal. The second and third harmonic of a 100-fs Ti:sapphire laser with a repetition rate of 80 MHz are used for excitation. The photon energy is set to 2.9 eV in the case of CdS and to 4.1 eV for both other samples. The PL was spectrally and temporally dispersed in a standard streak camera setup,[38] obtaining resolutions of 0.4 nm and 5 ps, respectively. The phonon-sideband emission from the samples was studied as a function of lattice temperature and carrier density.

IV. RESULTS AND DISCUSSION

The time-integrated PL spectra of the CdS (a) and the ZnO (b) samples are shown in Fig. 2 at two different lattice temperatures of 10 K and 90 K in the spectral range of the first two PSBs. The well-known polariton propagation in bulk crystals leads to a strong dependence of the near band-edge PL on surface properties.[13] Therefore, we neglect the zero phonon line (ZPL) in our analysis and subtract it from the measured spectra. The data are then normalized to the PL of the second PSB for better comparison. As expected, the observed sidebands are shifted to lower energies with respect to the free exciton transitions at 2.553 eV and 3.378 eV in CdS and ZnO, respectively. The corresponding spectral intervals are multiples of LO-phonon energies of 38 meV in CdS and 72 meV in ZnO.[40] Additional weak signatures in the 10 K spectrum of the ZnO sample are identified as PSBs of donor-bound excitons.[41] Time resolved PL traces of the PSB_2 emission are shown in the insets of Fig. 1(a) and 1(b). The incident photon flux at the sample surface is set to $n_0 = 10^{11}$ photons/cm^2 per pulse. Taking into account the pump geometry and the absorption coefficients,[13,40] this corresponds to initially injected carrier densities of 3×10^{15} cm^{-3} and 2×10^{15}cm^{-3} for ZnO and CdS, respectively. All values are well below the respective Mott densities,[13,42] thus favoring the formation of excitons. In both samples, the emission dynamics

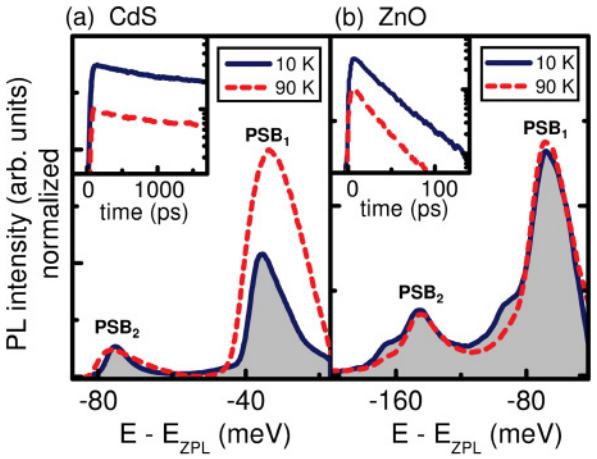

FIG. 2. (Color online) Time-integrated PL spectra of the first and the second PSB in CdS (a) and ZnO (b) at lattice temperatures of 10 K and 90 K. The inset shows the emission dynamics of the second PSB. The excitation density was $n_0 = 10^{11}$ photons/cm^2 per pulse.

are almost single exponential and do not change significantly with rising temperature. The data thus confirms exciton-related PL[13] and excludes thermal activation of additional recombination channels.

Our measurements clearly show that the ratio between the second and the first PSB strongly decreases in CdS, while it remains almost constant in ZnO when increasing the lattice temperature from 10 to 90 K. To quantify these differences, the measured temperature dependence of the PSB_2/PSB_1 intensity ratios for ZnO, ZnS, and CdS are plotted in Fig. 3(a). The corresponding theoretical results in Fig. 3(b) are obtained by calculating the contributions of Fröhlich and deformation-potential coupling. The comparison clearly shows that Fröhlich coupling dominates PSB scattering in CdS, whereas ZnO has the deformation potential coupling as the main exciton–phonon scattering process. At the same time, ZnS constitutes an intermediate case where both mechanisms equally contribute to the PSB emission.

Our findings are corroborated by the pump power dependence of the PSB luminescence. The carrier temperature rises for increasing excitation densities due to the formation of a nonequilibrium phonon population, leading to the well-known hot-phonon effect.[2] This provides an alternative way to alter the exciton distribution in favor of higher **k** values, i.e., momenta. Figure 4(a) shows the PSB_2/PSB_1 intensity ratios for ZnO (circles) and CdS (triangles) at 10 K as a function of excitation power. The resulting carrier density for the highest power applied is below 1×10^{18} cm^{-3} and, thus, still does not exceed the Mott density in both materials.[13,42] The PSB_2/PSB_1 ratio in ZnO increases only slightly for higher carrier densities. At the same time, the relative intensity of the second sideband decreases almost by a factor of two in the case of CdS. The pronounced density dependence of the PSB ratio therefore also influences the relative PL dynamics, see Figs. 4(b) and 4(c). The decay rates for the first and second PSB deviate from each other in the case of CdS [Fig. 4(c)] and are equal for the ZnO sample [Fig. 4(b)]. These results are fully consistent with temperature-dependent measurements, showing Fröhlich

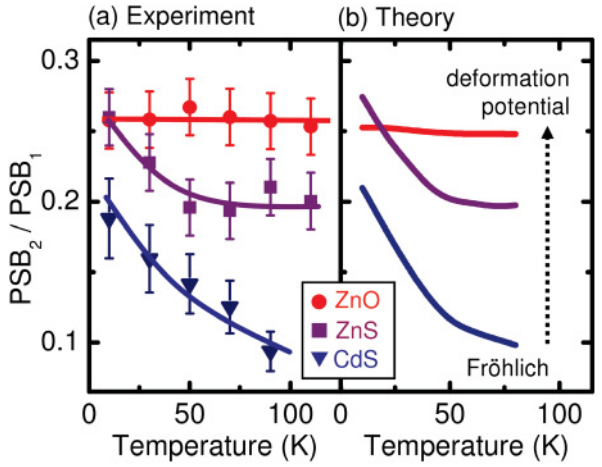

FIG. 3. (Color online) (a) Ratios of the second and first phonon sidebands as a function of lattice temperature for ZnO (circles), ZnS (squares), and CdS (triangles, top to bottom) for an excitation density of 10^{11} photons/cm^2 per pulse. The solid lines are given as guides to the eye. The corresponding results obtained from the many-body calculations are shown in (b).

behavior for the PSB emission in CdS and the deformation potential scattering in ZnO.

V. CONCLUSION

In conclusion, the exciton-phonon interaction mechanisms in polar semiconductors are studied theoretically and experimentally. A theoretical many-body approach is used to develop a straightforward way to identify the dominant scattering processes by the evaluation of phonon-assisted emission. The PSBs of ZnO, ZnS, and CdS are investigated by time-resolved PL spectroscopy as a function of temperature and excitation density. Fröhlich coupling governs the scattering in CdS, while deformation potential scattering turns out to be the dominant mechanism in ZnO. Both processes contribute about equally in ZnS. It is important to notice that our theory clearly shows that the scattering between a *single electron* and an optical phonon in all the studied cases is dominated by the Fröhlich interaction. However, particularly for ZnO, these contributions are suppressed by the strong Coulomb coupling of electrons and holes in excitons, rendering deformation potential scattering the overall dominant mechanism responsible for the sideband emission.

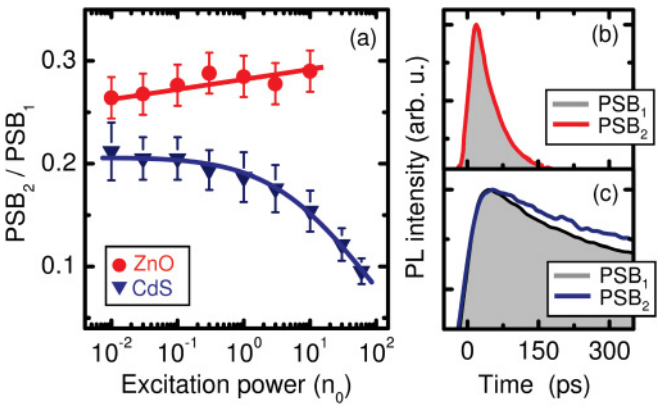

FIG. 4. (Color online) (a) Ratio of the second and first phonon sidebands as a function of excitation density at $T = 10$ K for ZnO (circles) and CdS (full triangles). Solid lines are guides to the eye. n_0 corresponds to the photon flux of 10^{11} photons/cm^2 per pulse. Normalized transients for ZnO (b) and CdS (c) of the first and second PSB are shown by solid lines and gray areas, respectively.

ACKNOWLEDGMENTS

A.C. and S.C. acknowledge helpful discussions with W. W. Rühle. Financial support by the German Science Foundation (DFG) and the German Ministry for Education and Research (BMBF) is gratefully acknowledged. C.B. thanks the International Research Training Group 790 *Electron-Electron Interactions in Solids* (Marburg-Budapest) for financial support.

APPENDIX: LOW-DENSITY EXCITON-DOMINATED PHONON SIDEBANDS

The description of phonon sideband luminescence is presented in Refs. 43 and 44 using the polaron picture and in Ref. 39 using the electron-hole picture. Within the applied theoretical approach, the semiconductor system as well as the carrier-carrier Coulomb-interaction and light-matter coupling mechanisms are treated microscopically using a quantized continuum model for the phonons. Both polaron and electron-hole treatments become rather cumbersome when resonances beyond the first sideband are evaluated. Therefore, we study here exciton-population dominated PSB_1 and PSB_2 when carrier densities are low. In this limiting case, we may start from a simplified system Hamiltonian

$$H = H_{\mathrm{X}} + H_{\mathrm{vib}} + H_{\mathrm{em}} + H_{\mathrm{X-vib}} + H_{\mathrm{X-em}}, \tag{A1}$$

where the noninteracting part contains

$$H_{\mathrm{X}} = \sum_{\nu,\mathbf{q}} E_{\nu,\mathbf{q}} X^{\dagger}_{\nu,\mathbf{q}} X_{\nu,\mathbf{q}}, \tag{A2}$$

with exciton operator $X_{\nu,\mathbf{q}}$ identified by state index ν and center-of-mass momentum $\hbar\mathbf{q}$. For elevated densities, H_{X} must be supplemented with additional pure carrier contributions,[37] and they can be ignored only at low densities. The free phonons and photons are described by

$$H_{\mathrm{vib}} = \sum_{\mathbf{p}} \hbar\Omega_{\mathrm{LO}} \left(D^{\dagger}_{\mathbf{p}} D_{\mathbf{p}} + \tfrac{1}{2} \right) \tag{A3}$$

and

$$H_{\mathrm{em}} = \sum_{\mathbf{q}} \hbar\omega_{\mathbf{q}} \left(B^{\dagger}_{\mathbf{q}} B_{\mathbf{q}} + \tfrac{1}{2} \right), \tag{A4}$$

where $\hbar\Omega_{\mathrm{LO}}$ is the LO-phonon energy and $\omega_{\mathbf{q}}$ sets the photon dispersion. Like always, phonon $D_{\mathbf{p}}$ and photon $B_{\mathbf{q}}$ are bosonic, while $X_{\nu,\mathbf{q}}$ is bosonic only approximately. For the low-density study performed here, we apply the bosonic approximation

$$[X_{\nu,\mathbf{Q}}, X^{\dagger}_{\nu',\mathbf{Q}'}]_- = \delta_{\nu,\nu'}\delta_{\mathbf{Q},\mathbf{Q}'}, \tag{A5}$$

$$[X_{\nu,\mathbf{Q}}, X_{\nu',\mathbf{Q}'}]_- = 0 = [X^{\dagger}_{\nu,\mathbf{Q}}, X^{\dagger}_{\nu',\mathbf{Q}'}]_-. \tag{A6}$$

In this situation, the exciton-phonon and exciton-photon interactions are described by

$$H_{\mathrm{X-vib}} = \sum_{\nu,\nu'} \sum_{\mathbf{Q},\mathbf{p}} G_{\mathbf{p}}^{\nu,\nu'} X_{\nu,\mathbf{Q}-\mathbf{p}}^{\dagger} X_{\nu',\mathbf{Q}} (D_{-\mathbf{p}} + D_{\mathbf{p}}^{\dagger}), \quad \text{(A7)}$$

$$H_{\mathrm{X-em}} = -\sum_{\nu,\mathbf{q}} \mathrm{i}[\mathcal{F}_{\nu,\mathbf{q}} X_{\nu,\mathbf{q}}^{\dagger} + \mathcal{F}_{\nu,\mathbf{q}}^{\star} X_{\nu',\mathbf{q}}] B_{\mathbf{q}} + \mathrm{h.c.}, \quad \text{(A8)}$$

respectively, where $G_{\mathbf{p}}^{\nu,\nu'}$ and $\mathcal{F}_{\nu,\mathbf{q}}$ determine exciton-phonon and exciton-light coupling matrix elements, respectively.

Computing the Heisenberg equation of motion, the incoherent photon flux follows from

$$I_{\mathrm{PL}}(\omega) = \frac{\partial}{\partial t} \Delta \langle B_{\mathbf{q}}^{\dagger} B_{\mathbf{q}} \rangle = \frac{2}{\hbar} \mathrm{Re}\Big[\sum_{\nu} \mathcal{F}_{\nu,\mathbf{q}}^{\star} \Pi_{\nu,\mathbf{q}}^{(0)} \Big]. \quad \text{(A9)}$$

This equation contains the photon-assisted polarization $\Pi_{\nu,\mathbf{q}}^{(0)} \equiv \Delta \langle B_{\mathbf{q}}^{\dagger} X_{\nu,\mathbf{q}} \rangle$. The corresponding phonon-assisted recombination correlations are $\Pi_{\nu,\mathbf{q};\mathbf{p}_1,\ldots,\mathbf{p}_n}^{(n)} \equiv \Delta \langle D_{\mathbf{p}_n}^{\dagger} \cdots D_{\mathbf{p}_1}^{\dagger} B_{\mathbf{q}}^{\dagger} X_{\nu,\mathbf{q}+\mathbf{p}_{1,n}} \rangle$, where $\mathbf{p}_{1,n} \equiv \sum_{j=1}^{n} \mathbf{p}_j$ is introduced to shorten the notation. The general equation of motion for $\Pi^{(n)}$ follows from

$$\begin{aligned} \mathrm{i}\hbar \frac{\partial}{\partial t} \Pi_{\nu,\mathbf{q};\mathbf{p}_1,\ldots,\mathbf{p}_n}^{(n)} &= (E_{\nu,\mathbf{q}+\mathbf{p}_{1,n}} - \hbar\omega_{\mathbf{q}} - n\hbar\Omega_{\mathrm{LO}})\, \Pi_{\nu,\mathbf{q};\mathbf{p}_1,\ldots,\mathbf{p}_n}^{(n)} \\ &\quad + \mathrm{i} \sum_{\nu'} \mathcal{F}_{\nu',\mathbf{q}}\, \Delta \big\langle D_{\mathbf{p}_n}^{\dagger} \cdots D_{\mathbf{p}_1}^{\dagger} X_{\nu',\mathbf{q}}^{\dagger} X_{\nu,\mathbf{q}+\mathbf{p}_{1,n}} \big\rangle \\ &\quad + \sum_{\nu',\mathbf{p}} G_{\mathbf{p}}^{\nu,\nu'}\, \Pi_{\nu',\mathbf{q};\mathbf{p},\mathbf{p}_1,\ldots,\mathbf{p}_n}^{(n+1)}. \end{aligned} \quad \text{(A10)}$$

Equations (A9) and (A10) have the structure of the *semiconductor luminescence equations*.[37] As an additional feature, phonon-assisted processes are now also included.

To solve ZPL, PSB_1, and PSB_2, we need to solve Eq. (A10) for $n = 0, 1$, and 2, respectively:

$$\begin{aligned} \mathrm{i}\hbar \frac{\partial}{\partial t} \Pi_{\nu,\mathbf{q}}^{(0)} &= (E_{\nu,\mathbf{q}} \Pi_{\nu,\mathbf{q}}^{(0)} - \hbar\omega_{\mathbf{q}} - \mathrm{i}\gamma^{(0)})\, \Pi_{\nu,\mathbf{q}}^{(0)} \\ &\quad + \mathrm{i}\mathcal{F}_{\nu,\mathbf{q}}^{\star}\, \Delta \langle X_{\nu,\mathbf{q}}^{\dagger} X_{\nu,\mathbf{q}} \rangle + \sum_{\nu',\mathbf{p}} G_{\mathbf{p}}^{\nu,\nu'}\, \Pi_{\nu',\mathbf{q};\mathbf{p}}^{(1)}, \end{aligned} \quad \text{(A11)}$$

$$\begin{aligned} \mathrm{i}\hbar \frac{\partial}{\partial t} \Pi_{\nu,\mathbf{q};\mathbf{p}_1}^{(1)} &= (E_{\nu,\mathbf{q}+\mathbf{p}_1} - \hbar\omega_{\mathbf{q}} - \hbar\Omega_{\mathrm{LO}} - \mathrm{i}\gamma^{(1)})\, \Pi_{\nu,\mathbf{q};\mathbf{p}_1}^{(1)} \\ &\quad + \mathrm{i} \sum_{\nu'} \mathcal{F}_{\nu',\mathbf{q}}^{\star}\, \Delta \big\langle D_{\mathbf{p}_1}^{\dagger} X_{\nu',\mathbf{q}}^{\dagger} X_{\nu,\mathbf{q}+\mathbf{p}_1} \big\rangle \\ &\quad + \sum_{\nu',\mathbf{p}} G_{\mathbf{p}}^{\nu,\nu'}\, \Pi_{\nu',\mathbf{q};\mathbf{p},\mathbf{p}_1}^{(2)}, \end{aligned} \quad \text{(A12)}$$

$$\begin{aligned} \mathrm{i}\hbar \frac{\partial}{\partial t} \Pi_{\nu,\mathbf{q};\mathbf{p}_1,\mathbf{p}_2}^{(2)} &= (E_{\nu,\mathbf{q}+\mathbf{p}_1} - \hbar\omega_{\mathbf{q}} - 2\hbar\Omega_{\mathrm{LO}} - \mathrm{i}\gamma^{(2)})\, \Pi_{\nu,\mathbf{q};\mathbf{p}_1,\mathbf{p}_2}^{(2)} \\ &\quad + \mathrm{i} \sum_{\nu'} \mathcal{F}_{\nu',\mathbf{q}}^{\star}\, \Delta \big\langle D_{\mathbf{p}_2}^{\dagger} D_{\mathbf{p}_1}^{\dagger} X_{\nu',\mathbf{q}}^{\dagger} X_{\nu,\mathbf{q}+\mathbf{p}_1+\mathbf{p}_2} \big\rangle, \end{aligned} \quad \text{(A13)}$$

where we have added dephasing $\gamma^{(n)}$ to describe scattering processes phenomenologically. For elevated densities, a $f^{\mathrm{e}} f^{\mathrm{h}}$ source also appears, giving rise to plasma-initiated emission at the excitonic ZPL and PSB_n resonances, c.f. Ref. 38.

The spontaneous-emission source terms that appear in Eqs. (A11)–(A13) take the form

$$\begin{aligned} \mathrm{i}\hbar \frac{\partial}{\partial t} \big\langle D_{\mathbf{p}_n}^{\dagger} \cdots D_{\mathbf{p}_1}^{\dagger} X_{\nu',\mathbf{q}}^{\dagger} X_{\nu,\mathbf{q}+\mathbf{p}_{1,n}} \big\rangle &= \big[E_{\nu,\mathbf{q}+\mathbf{p}_{1,n}} - E_{\nu',\mathbf{q}} - n\hbar\Omega_{\mathrm{LO}} - \mathrm{i}\eta_{\mathrm{X}}^{(n)} \big] \big\langle D_{\mathbf{p}_n}^{\dagger} \cdots D_{\mathbf{p}_1}^{\dagger} X_{\nu',\mathbf{q}}^{\dagger} X_{\nu,\mathbf{q}+\mathbf{p}_{1,n}} \big\rangle - \sum_{\nu'',\nu'''} \sum_{\mathbf{Q}} \sum_{j=1}^{n} \big(G_{\mathbf{p}_j}^{\nu''',\nu''} \big)^{\star} \\ &\quad \times \Big\langle \Big(\prod_{i \neq j}^{n} D_{\mathbf{p}_j}^{\dagger} \Big) X_{\nu'',\mathbf{Q}+\mathbf{p}_j}^{\dagger} X_{\nu''',\mathbf{Q}} X_{\nu',\mathbf{q}}^{\dagger} X_{\nu,\mathbf{q}+\mathbf{p}_{1,n}-\mathbf{p}_j} \Big\rangle \sum_{\nu''} \sum_{\mathbf{Q}} \big\langle D_{\mathbf{p}_n}^{\dagger} \cdots D_{\mathbf{p}_1}^{\dagger} (D_{\mathbf{Q}}^{\dagger} + D_{-\mathbf{Q}}) \\ &\quad \times \big[G_{\mathbf{Q}}^{\nu,\nu''} X_{\nu',\mathbf{q}}^{\dagger} X_{\nu'',\mathbf{q}+\mathbf{Q}+\mathbf{p}_{1,n}} - \big(G_{-\mathbf{Q}}^{\nu',\nu''} \big)^{\star} X_{\nu',\mathbf{q}-\mathbf{Q}}^{\dagger} X_{\nu,\mathbf{q}+\mathbf{p}_{1,n}} \big] \big\rangle, \end{aligned} \quad \text{(A14)}$$

where we again have added a dephasing $\eta_{\mathrm{X}}^{(n)}$ for each replica. We only consider those contributions to a given replica that are of the lowest order in the electron-phonon coupling constants. Therefore, we can neglect the last line of Eq. (A14) in the following analysis. Applying the cluster-expansion scheme[37,45–49] and solving Eq. (A14) in steady state, we obtain the form for phonon sidebands of arbitrary order

$$\begin{aligned} \big\langle D_{\mathbf{p}_n}^{\dagger} \cdots D_{\mathbf{p}_1}^{\dagger} X_{\nu',\mathbf{q}}^{\dagger} X_{\nu,\mathbf{q}+\mathbf{p}_{1,n}} \big\rangle &= \sum_{\mu_1,\ldots,\mu_{n-1}} \sum_{j_1=1}^{n} \sum_{\substack{j_2=1 \\ j_2 \neq j_1}}^{n} \cdots \sum_{\substack{j_n=1 \\ j_n \neq j_1,\ldots,j_{n-1}}}^{n} \big(G_{\mathbf{p}_{j_1}}^{\nu',\mu_1} \big)^{\star} \big(G_{\mathbf{p}_{j_2}}^{\mu_1,\mu_2} \big)^{\star} \cdots \big(G_{\mathbf{p}_{j_n}}^{\mu_{n-1},\nu} \big)^{\star} \Delta N_{\nu,\mathbf{q}+\mathbf{p}_{1,n}} \\ &\quad \times \Big\{ \prod_{l=1}^{n} \big[E_{\nu,\mathbf{q}+\mathbf{p}_{1,n}} - E_{\mu_l,\mathbf{q}+\mathbf{p}_{j_1,j_l}} - l\hbar\Omega_{\mathrm{LO}} - \mathrm{i}\eta_{\mathrm{X}}^{(l)} \big] \Big\}^{-1}, \end{aligned} \quad \text{(A15)}$$

where we set $\mu_n = \nu'$. This expression identifies the exciton population

$$\Delta \langle X_{\nu,\mathbf{q}}^{\dagger} X_{\nu,\mathbf{q}} \rangle = \Delta N_{\nu,\mathbf{q}} \quad \text{(A16)}$$

as the source for the ZPL. In the same way, we find the PSB_1 and PSB_2 sources

$$\Delta\langle D^\dagger_{\mathbf{p}_1} X^\dagger_{\nu',\mathbf{q}} X_{\nu,\mathbf{q}+\mathbf{p}_1}\rangle = \frac{\left(G^{\nu',\nu}_{\mathbf{p}_1}\right)^\star \Delta N_{\nu,\mathbf{q}+\mathbf{p}_1}}{E_{\nu,\mathbf{q}+\mathbf{p}_1} - E_{\nu',\mathbf{q}} - \hbar\Omega_{\mathrm{LO}} - \mathrm{i}\eta^{(1)}_{\mathrm{X}}} \tag{A17}$$

and

$$\begin{aligned}\Delta\langle D^\dagger_{\mathbf{p}_2} D^\dagger_{\mathbf{p}_1} X^\dagger_{\nu',\mathbf{q}} X_{\nu,\mathbf{q}+\mathbf{p}_1+\mathbf{p}_2}\rangle &= \sum_\mu \frac{\Delta N_{\nu,\mathbf{q}+\mathbf{p}_1+\mathbf{p}_2}}{E_{\nu,\mathbf{q}+\mathbf{p}_1+\mathbf{p}_2} - E_{\nu',\mathbf{q}} - 2\hbar\Omega_{\mathrm{LO}} - \mathrm{i}\eta^{(2)}_{\mathrm{X}}} \\ &\times \left[\frac{\left(G^{\nu',\mu}_{\mathbf{p}_1}\right)^\star \left(G^{\mu,\nu}_{\mathbf{p}_2}\right)^\star}{E_{\nu,\mathbf{q}+\mathbf{p}_1+\mathbf{p}_2} - E_{\mu,\mathbf{q}+\mathbf{p}_1} - \hbar\Omega_{\mathrm{LO}} - \mathrm{i}\eta^{(1)}_{\mathrm{X}}} + \frac{\left(G^{\nu',\mu}_{\mathbf{p}_2}\right)^\star \left(G^{\mu,\nu}_{\mathbf{p}_1}\right)^\star}{E_{\nu,\mathbf{q}+\mathbf{p}_1+\mathbf{p}_2} - E_{\mu,\mathbf{q}+\mathbf{p}_2} - \hbar\Omega_{\mathrm{LO}} - \mathrm{i}\eta^{(1)}_{\mathrm{X}}}\right].\end{aligned} \tag{A18}$$

Respectively, these sources drive $\Pi^{(n)}$ as indicated in Eq. (A10). We see that $\Pi^{(0)}$ is coupled to $\Pi^{(1)}$ and $\Pi^{(2)}$. As we determine the steady state, we can determine the steady-state spectra (6), (13), and (14) defining ZPL, PSB_1, and PSB_2 spectra when the analysis includes $1s$ and $2p$ states. It is numerically confirmed that these contributions dominate the spectra under the conditions studied.

[1] R. P. Stanley, J. Hegarty, R. Fischer, J. Feldmann, E. O. Göbel, R. D. Feldman, and R. F. Austin, Phys. Rev. Lett. **67**, 128 (1991).

[2] *Hot Electrons in Semiconductors: Physics and Devices*, edited by N. Balkan (Clarendon Press, Oxford, 1998).

[3] T. Kampfrath, L. Perfetti, F. Schapper, C. Frischkorn, and M. Wolf, Phys. Rev. Lett. **95**, 187403 (2005).

[4] U. Woggon, F. Gindele, O. Wind, and C. Klingshirn, Phys. Rev. B **54**, 1506 (1996).

[5] H. Zhao, S. Moehl, and H. Kalt, Phys. Rev. Lett. **89**, 097401 (2002).

[6] P. Borri, W. Langbein, S. Schneider, U. Woggon, R. L. Sellin, D. Ouyang, and D. Bimberg, Phys. Rev. Lett. **87**, 157401 (2001).

[7] Y.-Z. Ma, M. W. Graham, G. R. Fleming, A. A. Green, and M. C. Hersam, Phys. Rev. Lett. **101**, 217402 (2008).

[8] J. Brandt, P. Felbier, D. Fröhlich, C. Sandfort, M. Bayer, and H. Stolz, Phys. Rev. B **81**, 155214 (2010).

[9] H. Froehlich, Adv. Phys. **3**, 325 (1954).

[10] H. Haken, *Quantenfeldtheorie des Festkoerpers* (Teubner, Stuttgart, 1973).

[11] F. Giustino, M. L. Cohen, and S. G. Louie, Nature (London) **452**, 975 (2008).

[12] P. Yu and M. Cardona, *Fundamentals of Semiconductors: Physics and Material Properties*, 3rd ed. (Springer-Verlag, Berlin, Heidelberg, New York, 2005).

[13] C. F. Klingshirn, *Semiconductor optics*, 2nd ed. (Springer, Berlin Heidelberg New York, 2007).

[14] W.-K. Hong, G. Jo, M. Choe, T. Lee, J. I. Sohn, and M. E. Welland, Appl. Phys. Lett. **94**, 043103 (2009).

[15] A. W. E. Minnaert, A. Y. Silov, W. van der Vleuten, J. E. M. Haverkort, and J. H. Wolter, Phys. Rev. B **63**, 075303 (2001).

[16] T. Itoh, M. Nishijima, A. I. Ekimov, C. Gourdon, A. L. Efros, and M. Rosen, Phys. Rev. Lett. **74**, 1645 (1995).

[17] S. J. Xu, S.-J. Xiong, and S. L. Shi, J. Chem. Phys. **123**, 221105 (2005).

[18] H. Haug and S. W. Koch, *Quantum Theory of the Optical and Electronic Properties of Semiconductors*, 5th ed. (World Scientific, Singapore, 2009).

[19] S. Blumstengel, S. Sadofev, C. Xu, J. Puls, and F. Henneberger, Phys. Rev. Lett. **97**, 237401 (2006).

[20] K. Minoshima, M. Taiji, K. Misawa, and T. Kobayashi, Phys. Chem. Lett. **218**, 67 (1994).

[21] S. J. Xu, W. Liu, and M. F. Li, Appl. Phys. Lett. **81**, 2959 (2002).

[22] V. Ursaki, I. Tiginyanu, V. Zalamai, V. Masalov, E. Samarov, G. Emelchenko, and F. Briones, J. Appl. Phys. **96**, 1001 (2004).

[23] B.-L. Gao, Y. Xiong, and S.-J. Xiong, Phys. Rev. B **74**, 235102 (2006).

[24] S. Sohai, Y. Alivov, Z. Fan, and M. Holtz, J. Appl. Phys. **108**, 053507 (2010).

[25] S. Nomura and T. Kobayashi, Phys. Rev. B **45**, 1305 (1992).

[26] A. V. Fedorov, A. V. Baranov, and K. Inoue, Phys. Rev. B **56**, 7491 (1997).

[27] V. M. Fomin, V. N. Gladilin, J. T. Devreese, E. P. Pokatilov, S. N. Balaban, and S. N. Klimin, Phys. Rev. B **57**, 2415 (1998).

[28] W. A. Harrison, Phys. Rev. **104**, 1281 (1956).

[29] D. Braun, W. W. Rühle, C. Trallero-Giner, and J. Collet, Phys. Rev. Lett. **67**, 2335 (1991).

[30] C. Lange, N. S. Köster, S. Chatterjee, H. Sigg, D. Chrastina, G. Isella, H. von Känel, B. Kunert, and W. Stolz, Phys. Rev. B **81**, 045320 (2010).

[31] C. W. Litton, D. C. Reynolds, T. C. Collins, and Y. S. Park, Phys. Rev. Lett. **25**, 1619 (1970).

[32] S. Permogorov, *Excitons* (North-Holland, Amsterdam, 1982), pp. 177–203.

[33] I. V. Bondarev, S. A. Maksimenko, G. Y. Slepyan, I. L. Krestnikov, and A. Hoffmann, Phys. Rev. B **68**, 073310 (2003).

[34] K. Reimann, R. A. Kaindl, and M. Woerner, Phys. Rev. B **65**, 045302 (2001).

[35] W. Pötz and P. Vogl, Phys. Rev. B **24**, 2025 (1981).

[36] S.-H. Park and S.-L. Chuang, J. Appl. Phys. **87**, 353 (2000).

[37] M. Kira, F. Jahnke, W. Hoyer, and S. W. Koch, Prog. Quant. Electron. **23**, 189 (1999).

[38] A. Chernikov, T. Feldtmann, S. Chatterjee, M. Koch, M. Kira, and S. W. Koch, Sol. Stat. Comm. **150**, 1733 (2010).

[39] T. Feldtmann, *Influence of Phonons on Semiconductor Quantum Emission*, Ph.D. thesis, Fachbereich Physik, Philipps-Universität Marburg, Germany, 2009.

[40] O. Madelung, *Landolt-Boernstein: Numerical Data and Functional Relationships in Science and Technology* (Springer, Berlin Heidelberg New York, 1982).

[41]B. K. Meyer, H. Alves, D. M. Hofmann, W. Kriegseis, D. Forster, F. Bertram, J. Christen, A. Hoffmann, M. Straßburg, M. Dworzak, U. Haboeck, and A. V. Rodina, Phys. Status Solidi B **241**, 231 (2004).
[42]C. Klingshirn and H. Haug, Phys. Rep. **70**, 315 (1981).
[43]T. Feldtmann, M. Kira, and S. W. Koch, Phys. Status Solidi B **246**, 332 (2009).
[44]T. Feldtmann, M. Kira, and S. W. Koch, J. Lumin. **130**, 107 (2010).
[45]M. Kira and S. W. Koch, Phys. Rev. A **78**, 022102 (2008).
[46]J. Čížek, J. Chem. Phys. **45**, 4256 (1966).
[47]G. D. Purvis III and R. J. Bartlett, J. Chem. Phys. **76**, 1910 (1982).
[48]J. Fricke, Ann. Phys. **252**, 479 (1996).
[49]H. Wyld Jr. and B. Fried, Ann. Phys. **23**, 374 (1963).